A New Composite Reservoir Model for Thermal Well Test Analysis

Ashkan Jahanbani G.[#1], Tom A. Jelmert[#2]

[#1,2] *Department of Petroleum Engineering and Applied Geoscience, Norwegian University of Science and Technology (NTNU)*
S.P. Andersens vei 15 A, 7491 Trondheim, Norway

Abstract— **A composite reservoir may occur during any enhanced oil recovery project like steam injection into an oil reservoir. Falloff test analysis in steam injection projects offers a quick way to obtain estimates of the swept volume and steam zone properties. Most of the models used for the analysis assume two-region composite reservoirs with different but uniform properties separated by a sharp vertical interface, which is not very realistic. Strange trends seen on the pressure plots and the errors associated with the volume estimates could be related to the simplifying assumptions of the conventional models. The main objective of this paper is to develop a new analytical model for pressure transient analysis to improve previous results with inclusion of more realistic assumptions. The proposed model is a three-region composite model with an intermediate region in which mobility and storativity decrease as power law functions of the radial distance from the front. The fronts are considered to be tilted due to gravity effects. Steam condensation in the form of heat loss from the steam zone is also included in the analytical model. The new sets of type curves for well test interpretation are generated and verified. Effects of several parameters on the shape of type curves are discussed. The developed model can improve estimations of reservoir parameters using type curve matching and explain the anomalies seen on the data, which cannot be described using the conventional models. The general nature of the model makes it applicable to other types of composite reservoirs created either naturally or artificially.**

Keywords— **composite reservoir, gravity effect, heat loss, intermediate region, power-law variation, well test analysis**

I. INTRODUCTION

Steam injection enhances the recovery of oil by reducing the viscosity of mobile or immobile oil, causing chemical reactions and desired phase behaviour. Monitoring of swept volume over time is very important for assessing the success of any flooding project. It is used in thermal projects to estimate cumulative heat losses and thermal efficiencies. Thermal falloff test analysis offers a quick way to obtain an estimate of the swept volume. It can also provide an estimate of flow capacity and skin factor and is used for reservoir characterization.

Selection of the proper model is very important in well test analysis. A composite reservoir is usually formed by applying enhanced oil recovery (EOR) methods like steam injection into an oil reservoir. Radial composite reservoirs have gain attention since early 1960's (for instance in [1]).

Estimation of steam zone properties and swept volume from falloff test data is mostly based on the composite reservoir model with two regions having highly contrasting fluid mobilities, developed in [2]. This method is also called the pseudo-steady-state (PSS) method since the swept zone behaves as a closed reservoir for a short duration.

Several investigators noticed that the interface separating the two regions is not sharp. Instead, they assumed an intermediate region between the inner and outer regions, which is characterized by a rapid decline in mobility and storativity. This issue motivated further study of this subject area to be able to model the thermal process more realistically. Different three-region composite reservoir models were developed, thereafter ([3]-[5]). In these models, the intermediate region is represented by a uniform set of mobility and storativity values that lie between those in the inner and the outer region.

To represent secondary recovery processes even more realistically, analytical multi-region composite reservoir models have been proposed ([6]-[8]). Reference [9] used a multi-region composite reservoir model to study the effect of various trends of mobility and storativity variations on thermal well test data. The regions between the first and the last make up the intermediate region. This region is represented by a series of mobility and storativity values that decrease as some step functions of distance from the wellbore.

The concept of fractal geometry was used in a number of analytical models of pressure transient analysis of heterogeneous reservoirs to describe a fracture network. Extending this concept to composite reservoirs, a two-region composite reservoir model was presented in [10], where the inner region was assigned a fractal property (declining porosity and permeability with distance from the wellbore in a power law fashion), while the outer region was homogeneous.

Reference [11] shows an infinite two-region radial composite reservoir model for thermal recovery processes. In this model, the outer region is assigned a fractal property to represent the rapid decline of diffusivity due to the rapid decline in temperature ahead of the flood front. Reference [12] further used the fractal concept for property variation in the intermediate region in the development of a three-region composite reservoir model with vertical fronts to account for gradual changes of properties.

To best of our knowledge, not much analytical work has been done in this field recently. Analytical research has been done considering temperature transient analysis and condensation model (e.g. [13] and [14]). According to [15], a few works considered the phenomenon of gravity override and heat loss in oil reservoirs. However, all these studies treat the thermal recovery based on the previous methods and the models are two or three-region composite reservoirs. So, nothing much was added to the pre-existing knowledge.

Primary analysis of simulation studies of both vertical and horizontal steam injection wells ([16]-[18]), were done to evaluate the applicability of thermal well test analysis method. Results showed that quite reasonable estimates were obtained.

However, there are still huge errors in volume estimations in some cases. In addition, some trends seen on the pressure plots cannot be explained using the existing models.

The existing models should be updated and some of the simplifying assumptions in these models should be investigated in more details. Therefore, a new analytical model for transient pressure behaviour is presented which will improve the previous models with inclusion of some parameters and more realistic assumptions. This model is a three-region composite reservoir with power law property variation in the intermediate region. This accounts for smooth changes in mobility and storativity ahead of the front. Steam condensation in the form of heat loss to the surroundings is included in the model. Heat loss can be very significant in some situations and cannot be overlooked. Another important phenomenon is steam override due to gravity effect. Instead of the conventional way of treating the gravity effect, that is assuming a multi-layer reservoir model, a continuous tilted front is assumed over the entire reservoir thickness.

After validation of the model, a sensitivity analysis of the proposed model to the parameters included in the model, like heat loss coefficient, intermediate region properties and gravity effect, is done using the pressure derivative responses.

II. MATHEMATICAL MODEL

Some of the drawbacks of the conventional models of composite reservoirs were identified. In this section, development of a new mathematical model is thoroughly described. The following assumptions are used in the derivation:

1) Slightly compressible fluid (constant compressibility)
2) Isotropic porous medium of uniform thickness
3) Small pressure gradient
4) Single-phase radial flow
5) Applicability of Darcy's law
6) Negligible gravity and capillary inside different regions
7) Stationary fronts of infinitesimal thickness.

In this model, a single injector is located at the center of the reservoir. In addition to the assumptions named above, the injection time is assumed to be large compared to the shut-in time, to be able to apply the stationary front hypothesis.

Following the work presented in [19] and [20], steam condensation resulting from the heat losses to the over- and underburdens is incorporated in the continuity equation. Assuming a three-region composite reservoir model (shown in Fig. 1), diffusivity equation for flow in the first region (here steam zone) can be written as:

$$\frac{1}{r}\frac{\partial}{\partial r}\left(r\frac{\partial p_1}{\partial r}\right) = \frac{(\varphi c_t)_1}{\left(\frac{k}{\mu}\right)_1}\frac{\partial p_1}{\partial t} + G\frac{(Fe-1)}{\left(\frac{k}{\mu}\right)_1} \tag{1}$$
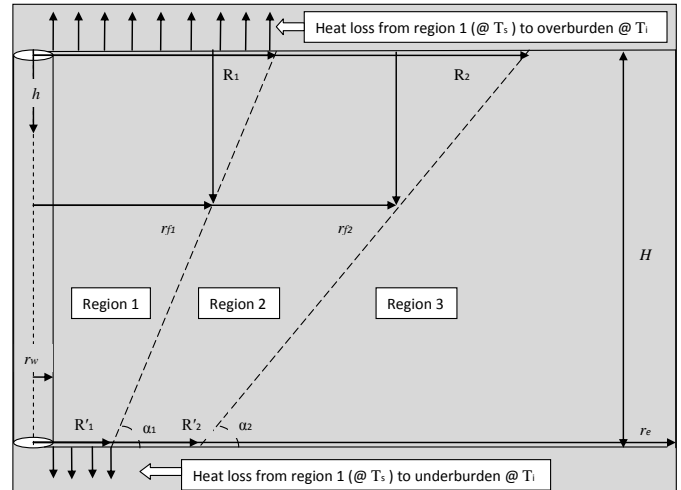

Fig. 1 Representation of the 3-region composite reservoir model with tilted fronts and heat loss effect ($r_{f1}=R_1-h\cot\alpha_1$, $r_{f2}=R_2-h\cot\alpha_2$)

G is the steam condensation rate per volume described in terms of the rate of heat loss from top and bottom bases of region 1 (the frustum of cone, Fig. 1) to the surroundings as:

$$G = \frac{\left(-K\frac{\partial T}{\partial z}|z=0 \times \pi R_1^2\right) + \left(-K\frac{\partial T}{\partial z}|z=H \times \pi \acute{R}_1^2\right)}{\frac{\pi}{3}\left(R_1^2 + \acute{R}_1^2 + R_1\acute{R}_1\right)H\rho_w L_V} \tag{2}$$

This expression is the modified form of G given in [19] for a cylindrical steam zone assuming identical heat loss from top and bottom of the cylinder. Explicit expression for heat loss is required to solve the diffusivity equation. The lower-bound expression for the heat loss [19] is applied since it can better approximate the fall-off test conditions:

$$-K\frac{\partial T}{\partial z}|z=0,H \cong \frac{K}{\sqrt{\pi\alpha}}\frac{(T_s - T_i)}{\sqrt{t}} \tag{3}$$

Lower-bound represents the case in which temperature assumes the constant value T_s as soon as the steam injection begins. The expression for G becomes:

$$G = \frac{3K}{\sqrt{\pi\alpha}}\frac{1}{H\rho_w L_V}\frac{(T_s - T_i)}{\sqrt{t}}\left(\frac{R_1^2 + \acute{R}_1^2}{R_1^2 + \acute{R}_1^2 + R_1\acute{R}_1}\right) \tag{4}$$

Flow in the second region is described by:

$$\frac{1}{r}\frac{\partial}{\partial r}\left(\left(\frac{k}{\mu}\right)_2 r\frac{\partial p_2}{\partial r}\right) = (\varphi c_t)_2 \frac{\partial p_2}{\partial t} \tag{5}$$

In this region unlike first and third regions, properties are not constant and are supposed to vary exponentially with the ratio of radial distance to the first front radius at any depth as:

$$\left(\frac{k}{\mu}\right)_2 = \frac{\left(\frac{k}{\mu}\right)_1}{M_{12}}\left(\frac{r}{r_{f1}}\right)^{-\theta 1}$$

In the same way, for storage in the second region:

$$(\varphi c_t)_2 = \frac{(\varphi c_t)_1}{F_{12}}\left(\frac{r}{r_{f1}}\right)^{-\theta 2}$$

M_{12} and F_{12} are mobility and storativity ratios, respectively, between fluids on the two sides of the first front.

The flow equation for the third region is:

$$\frac{1}{r}\frac{\partial}{\partial r}\left(\left(\frac{k}{\mu}\right)_3 r \frac{\partial p_3}{\partial r}\right) = (\varphi c_t)_3 \frac{\partial p_3}{\partial t} \tag{6}$$

Dimensionless parameters are defined as:

$$r_D = \frac{r}{r_w} \qquad\qquad t_D = \frac{\left(\frac{k}{\mu}\right)_1 t}{(\varphi c_t) r_w^2}$$

$$h_D = \frac{2\pi \left(\frac{k}{\mu}\right)_1 H}{qB}(\rho_1 g h) \qquad p_{wD} = \frac{2\pi \left(\frac{k}{\mu}\right)_1 H}{qB}(p_i - p_{wf})$$

$$p_{jD} = \frac{2\pi \left(\frac{k}{\mu}\right)_1 H}{qB}(p_i - p_j) \qquad j = 1,2,3$$

$$\varepsilon = \frac{qB}{2\pi \left(\frac{k}{\mu}\right)_1 H}\left(\frac{1}{\rho_1 g r_w}\right)$$

$$\beta = \frac{6\pi(Fe-1)K(T_s-T_i)r_w}{\rho_w L_V q B}\left(\frac{R_1^2+\hat{R}_1^2}{R_1^2+\hat{R}_1^2+R_1\hat{R}_1}\right)\left(\frac{\left(\frac{k}{\mu}\right)_1}{\pi\alpha(\varphi c_t)_1}\right)^{\frac{1}{2}}$$

Using the definitions provided above and substituting for the terms in equations 1, 5 and 6, after some manipulation they can be rewritten respectively as:

$$\frac{\partial^2 p_{1D}}{\partial r_D^2} + \frac{1}{r_D}\frac{\partial p_{1D}}{\partial r_D} = \frac{\partial p_{1D}}{\partial t_D} - \beta\frac{1}{\sqrt{t_D}}$$
$$1 < r_D < R_{1D} - \varepsilon\cot\alpha_1 h_D \tag{7}$$

$$\frac{\partial^2 p_{2D}}{\partial r_D^2} + \frac{1-\theta_1}{r_D}\frac{\partial p_{2D}}{\partial r_D} = \frac{M_{12}}{F_{12}}(R_{1D}-\varepsilon\cot\alpha_1 h_D)^{\theta_2-\theta_1}r_D^{\theta_1-\theta_2}\frac{\partial p_{2D}}{\partial t_D}$$
$$R_{1D} - \varepsilon\cot\alpha_1 h_D < r_D < R_{2D} - \varepsilon\cot\alpha_2 h_D \tag{8}$$

$$\frac{\partial^2 p_{3D}}{\partial r_D^2} + \frac{1}{r_D}\frac{\partial p_{3D}}{\partial r_D} = \frac{M_{13}}{F_{13}}\frac{\partial p_{3D}}{\partial t_D}$$
$$r_D > R_{2D} - \varepsilon\cot\alpha_2 h_D \tag{9}$$

The next step is to take Laplace of the differential equations whose solutions are applied to boundary conditions (described later) in order to form a set of equations and then solve them. Initially, the system is at equilibrium or at initial pressure. Taking Laplace of the initial condition results in:

$$\overline{p_{1D}} = \overline{p_{2D}} = \overline{p_{3D}} = 0 \qquad @ \ t_D = 0 \tag{10}$$

This is substituted in the Laplace of differential equations. After taking Laplace, equation 7 is written as:

$$\frac{\partial^2 \overline{p_{1D}}}{\partial r_D^2} + \frac{1}{r_D}\frac{\partial \overline{p_{1D}}}{\partial r_D} - s\left(\overline{p_{1D}} - \beta\frac{\sqrt{\pi}}{s^{3/2}}\right) = 0 \tag{11}$$

This is a modified Bessel equation and the solution is:

$$\overline{p_{1D}} = AI_0(\sqrt{s}\,r_D) + BK_0(\sqrt{s}\,r_D) + \beta\frac{\sqrt{\pi}}{s^{3/2}} \tag{12}$$

Taking the Laplace of equation 8 gives:

$$\frac{\partial^2 \overline{p_{2D}}}{\partial r_D^2} + \frac{1-\theta_1}{r_D}\frac{\partial \overline{p_{2D}}}{\partial r_D} - \frac{M_{12}}{F_{12}}(R_{1D}-\varepsilon\cot\alpha_1 h_D)^{\theta_2-\theta_1}r_D^{\theta_1-\theta_2}s\overline{p_{2D}} = 0 \tag{13}$$

Development of the solution to this equation is explained in Appendix A, in details. The final form of the solution is:

$$\overline{p_{2D}} = Cr_D^\gamma I_v(\xi\,r_D^{\,b}) + Dr_D^\gamma K_v(\xi\,r_D^{\,b}) \tag{14}$$

Finally, equation 9 is written as:

$$\frac{\partial^2 \overline{p_{3D}}}{\partial r_D^2} + \frac{1}{r_D}\frac{\partial \overline{p_{3D}}}{\partial r_D} - \frac{M_{13}}{F_{13}}s\overline{p_{3D}} = 0 \tag{15}$$

The solution will be:

$$\overline{p_{3D}} = EI_0\left(\sqrt{\frac{M_{13}}{F_{13}}s}\,r_D\right) + FK_0\left(\sqrt{\frac{M_{13}}{F_{13}}s}\,r_D\right) \tag{16}$$

Laplace of wellbore pressure is obtained by substituting $r_d=1$ in equation 12, assuming no wellbore storage and skin:

$$\overline{p_{wD}} = AI_0(\sqrt{s}) + BK_0(\sqrt{s}) + \beta\frac{\sqrt{\pi}}{s^{3/2}} \tag{17}$$

To solve the derived flow equations for different regions, boundary conditions are introduced now. Inner boundary condition is the injection at constant rate, which is written in dimensionless form as:

$$r_D\frac{\partial p_{1D}}{\partial r_D}\Big|(r_D = 1) = -1 \tag{18}$$

Interface equations are written by assuming the continuity of pressure (better to say flow potential since gravity effect is applied across the fronts) and flux across the fronts. Effect of gravity at the tilted fronts is included in the flow potential term as $\Phi = p - \rho g h$ where h is assumed positive downward. The continuity of flow potential across the first and second fronts is written respectively in dimensionless form as:

$$\int_0^{H_D}(p_{1D}+h_D)dh_D = \int_0^{H_D}\left(p_{2D}+\frac{1}{\delta_{12}}h_D\right)dh_D \tag{19}$$

$$\int_0^{H_D}\left(p_{2D}+\frac{1}{\delta_{12}}h_D\right)dh_D = \int_0^{H_D}\left(p_{3D}+\frac{1}{\delta_{13}}h_D\right)dh_D \tag{20}$$

Continuity of flux across the first and second fronts is written respectively (including the effect of gravity), in dimensionless from as:

$$M_{12}\int_0^{H_D}\left(\frac{\partial p_{1D}}{\partial r_D}-\frac{\tan\alpha_1}{\varepsilon}\right)dh_D = \int_0^{H_D}\left(\frac{\partial p_{2D}}{\partial r_D}-\frac{\tan\alpha_1}{\varepsilon\,\delta_{12}}\right)dh_D \tag{21}$$

$$M_{23}\int_0^{H_D}\left(\frac{\partial p_{2D}}{\partial r_D}-\frac{\tan\alpha_2}{\varepsilon\,\delta_{12}}\right)dh_D = \int_0^{H_D}\left(\frac{\partial p_{3D}}{\partial r_D}-\frac{\tan\alpha_2}{\varepsilon\,\delta_{13}}\right)dh_D \tag{22}$$

In these equations, δ is the density ratio between fluids on the two sides of the fronts.

The outer boundary condition is written for three different types of boundaries to include a wide range of applications to bounded and unbounded reservoirs:

1) Infinite-acting reservoir:

$$\lim_{r_D \to \infty} p_{3D} = 0 \qquad (23)$$

2) No-flow boundary:

$$\frac{\partial p_{3D}}{\partial r_D}|(r_D = r_{eD}) = 0 \qquad (24)$$

3) Constant-pressure boundary:

$$p_{3D} = 0 \quad @ \quad r_D = r_{eD} \qquad (25)$$

Taking the Laplace of the boundary condition equations and substituting for the pressure solutions obtained before in them, gives the system of equations as:

$$a_{11}A + a_{12}B = d_1$$
$$a_{21}A + a_{22}B + a_{23}C + a_{24}D = d_2$$
$$a_{33}C + a_{34}D + a_{35}E + a_{36}F = d_3$$
$$a_{41}A + a_{42}B + a_{43}C + a_{44}D = d_4$$
$$a_{53}C + a_{54}D + a_{55}E + a_{56}F = d_5$$
$$a_{65}E + a_{66}F = d_6$$

This can be written in matrix form as $aX=d$, with the coefficients a_{ij} and d_i defined in Appendix B and the unknown matrix (A to F). The system of equations is solved and the unknown matrix is used to express the pressure in different regions. Finding the unknowns A and B, wellbore pressure in Laplace space can be obtained by equation 17. To obtain the dimensionless wellbore pressure and pressure derivative, equation 17 is inverted numerically from Laplace space to real space by Stehfest algorithm [21]. Notice that equation 17 contains no wellbore storage or skin effect. To include these effects in the solution presented, [22] developed the problem as a convolution integral. This is solved to give the dimensionless wellbore pressure in Laplace space including wellbore storage and skin as:

$$\overline{p_{wD(S,CD)}} = \frac{s\,\overline{p_{wD}} + S}{s(1 + C_D s\,[s\,\overline{p_{wD}} + S])} \qquad (26)$$

This equation is again numerically inverted to calculate the dimensionless wellbore pressure and pressure derivative including wellbore storage and skin.

III. RESULTS AND DISCUSSION

A. Model Validation

The model developed in this work is validated against some of the well-known composite reservoir models in the literature. The new model will reproduce these conventional models by omitting some assumptions or setting values to the parameters in the model. Fig. 2 shows the perfect match with the model of [23] generated for a homogeneous reservoir with different values of C_D. This was obtained by assuming no heat loss and gravity (i.e. vertical front in the model) and assuming equal properties in different regions.
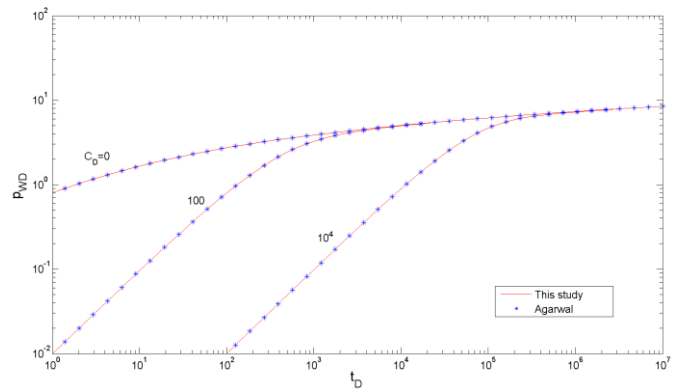

Fig. 2 Comparison of this study with homogeneous model of [23] for different values of C_D, S=0; R_D=1; M=1; F=1.

The model will reproduce the model of [12] (Fig. 3) by setting heat loss coefficient (β) to zero and the front angles to 90°. Reference [12] further verified the model against the model of [11] for an infinite two-region composite reservoir model with a fractal outer region. Pressure and pressure derivatives are shown in Fig. 3 for different sizes of the intermediate region. It can be observed that as the size of this region increases, the corresponding radial flow is established. This flow regime is identified by the stabilization of derivative at the middle time region.
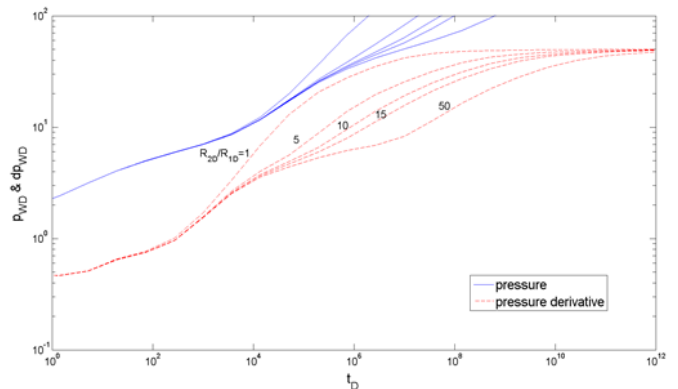

Fig. 3 Reproduction of the model of [12] showing the effect of size of the intermediate region, C_D=0; S=0; R_{1D}=100; M_{12}=10; M_{13}=100; F_{12}=1; F_{13}=1; θ_1=θ_2=1.

The model proposed in this work will reproduce many of the simpler single-layer two or three-region models as shown for instance in Figs. 4 and 5. The two-region composite models include [2] and [24] which will in turn generate other models. To generate the two-region models, R_{2D} is set equal to R_{1D} and fronts are assumed vertical. Again, θ_1 and θ_2 are set to zero to model constant properties in the two regions. Fig. 4 shows the derivative response for different values of storativity ratio between the two regions.
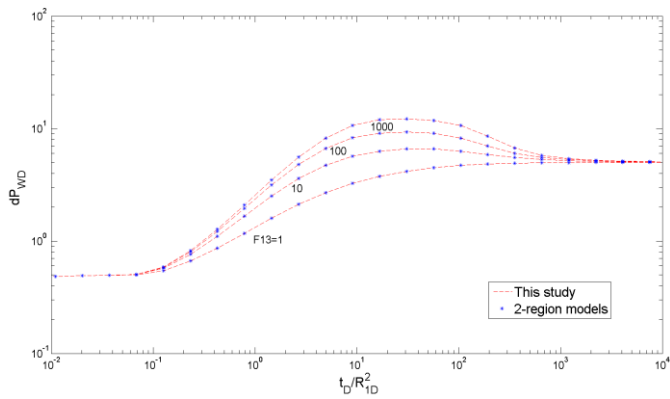
Fig. 4 Comparison of this study with 2-region composite reservoir models, $C_D=0$; $S=0$; $R_{1D}=R_{2D}=100$; $M_{12}=1$; $M_{13}=10$; $F_{12}=1$.

The model will further reduce to several three-region composite reservoir models such as in [5] and [24]. This is done if the exponents θ_1 and θ_2 are set to zero to model constant but different properties in the regions. Fig. 5 shows the perfect match for different mobility ratios.
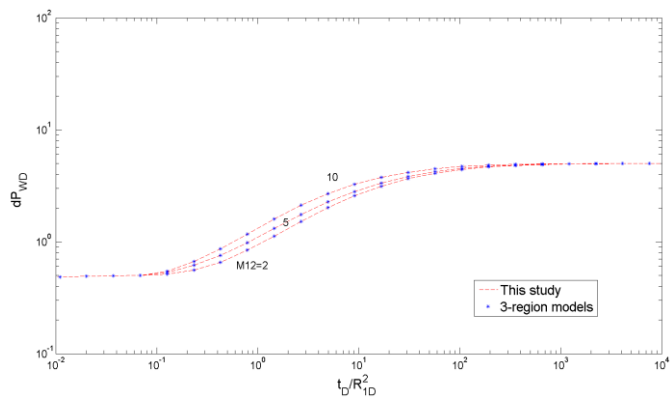

Fig. 5 Comparison of this study with 3-region composite reservoir models, $C_D=0$; $S=0$; $R_{1D}=100$; $R_{2D}=150$; $M_{13}=10$; $F_{12}=1$; $F_{13}=1$.

The model reproduces the model of [20] which was the starting point of this study regarding the heat loss analysis. Fig. 6 shows the model considering the effect of different values of heat loss coefficient, which is discussed in details later.
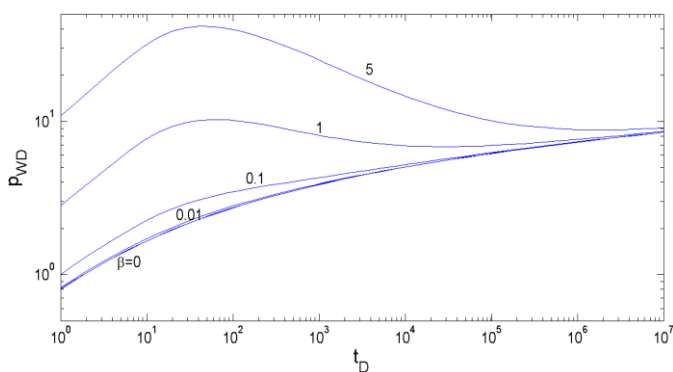

Fig. 6 Pressure behaviour for different values of heat loss coefficient, $C_D=0$; $S=0$; $R_D=10$; $M=1$; $F=1$.

Effect of gravity has been discussed in the literature using multi-layer models, for instance in [25]. Fig. 7 shows a good match between this study and the commingled multi-layer composite model of [25] with the front tilted at an angle of 60°. The multi-layer models may be improved by increasing number of layers or by adding the cross-flow between layers.
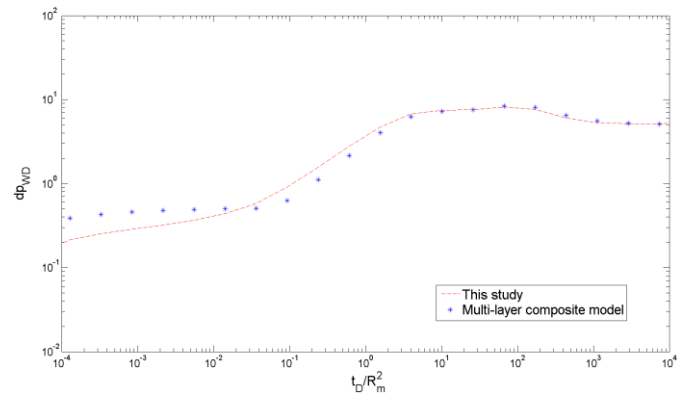

Fig. 7 Comparison of this study with multi-layer composite reservoir model of [25], $C_D=0$; $S=0$; $R_m=200$; $M=10$; $F=100$; $\alpha=60°$; $N=3$;

Therefore, the model presented in this study can be considered validated.

B. Effect of Different Model Parameters

After validating the model proposed in this paper against previous models, effects of some parameters used in the development of the model on the results are discussed in this section. Effects of the parameters such as mobility and storage ratios on the pressure behaviour were discussed in details in the literature (for instance in [5] and [24]). Value of M will affect the elevation of the constant derivative sections (radial flow) and F will affect the shape and occurrence of the hump of the transition between radial flow periods. Same conclusions are valid for the model developed in this work. Therefore, in the following sections, effects of the parameters included in the new model are investigated.

Unless mentioned, the following values are used in the development of the type curves:

$C_D=0$; $S=0$; $R_m=200$; $M_{12}=10$; $M_{13}=2000$; $F_{12}=10$; $F_{13}=1000$; $\alpha=60$; $\beta=0$; $H_D=0.55$; $\varepsilon=117$; $\theta_1=\theta_2=1$.

Notice that dp_{WD} refers to the logarithmic pressure derivative (i.e. $dp_{WD}/dlnt_D$). The initial 0.5 value of the derivative refers to the radial flow in the inner region, while the late time derivative stabilization refers to the radial flow in the outer region.

1) Effect of Heat Loss

The model presented in [20] included steam condensation in the flow model by considering heat loss from the steam zone to overburden and underburden. They modified the original solution to the composite reservoir model by including a term, which accounts for the heat loss and carried out a sensitivity study of the solution to this term. It was

concluded that under certain conditions, heat loss could have a significant effect on the pressure behavior and dominate the PSS period. Further analysis of heat loss was carried out in a previous work [18] and a modified method of analysis was proposed.

As suggested in [20] for a two-region model, Fig. 8 further confirms for the model presented in this study that for low values of β (0-0.1), shapes of the pressure and derivative curves are almost identical. At higher values of β (1-5), however, deviation happens due to significant heat loss. A half slope line on log-log plots of both pressure and derivative responses gradually appear which is characteristic of linear flow. This flow regime may mask the early and middle-time responses. This fact can be confirmed by investigating the radial and PSS flow equations in [18] or [20].
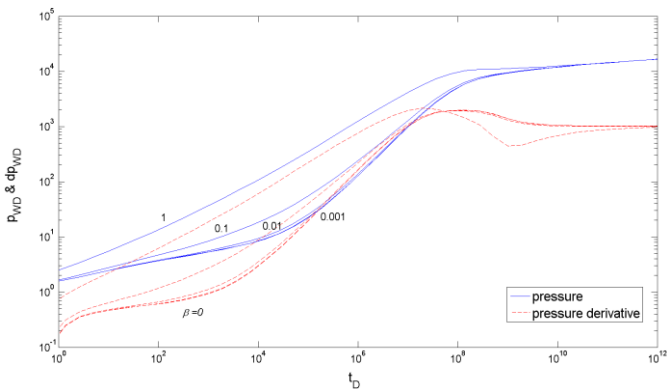

Fig. 8 Pressure and pressure derivative responses for different values of heat loss coefficient

Unlike the cases with small values of β for early time period, at higher β values the weight of the square root (linear flow) term in the pressure drop expression increases and will dominate the logarithmic (radial flow) term. The same thing happens to the PSS equation where at high values of β, linear flow term dominates the PSS behaviour. So, the effect of huge heat loss shows up as a linear flow trend, which may be misinterpreted as the linear flow due to the fractures induced by steam injection. This shows the importance of heat loss analysis and its inclusion in the well test model.

The effect is significant on the inner and intermediate region responses. Because of the huge mobility decrease in the outer region, mobility term will dominate the heat loss term and effect is not significant for the late time response as shown in Fig. 8. All the curves converge and form a single line at late times. However, for β values greater than 1, a minimum appears on derivative plot that delays the last derivative stabilization (start of the last radial flow).

2) Effect of Gravity

In some previous works (for instance in [25]), gravity was modeled using the concept of multi-layered reservoir models. This requires setting different values of radii to fronts at each layer. An alternative that was discussed in the development of the model in this study is to consider a continuous front tilted by an angle over the whole reservoir thickness. The expression for the front radius as a function of thickness (or depth) and front angle is implemented into the flow equations. Gravity term is added to the pressure and flux terms at the front locations to model the tilted front while the flow in the reservoir itself is assumed to be horizontal radial. As shown in Figs. 9 and 10, effect of gravity is discussed in terms of front angle and reservoir thickness.

Fig. 9 shows the derivative response for different front angles. The more the gravity effect (or smaller angle), the bigger the average front radius becomes and therefore pressure will diffuse for a longer period in the inner region resulting in a longer initial radial flow. In the case of significant gravity effect, unlike sharp vertical fronts, late time response is also affected since the second front is also tilted due to gravity effect. This may give rise to the last radial flow derivative plot. The occurrence of the transition hump and the last radial flow may also be delayed.
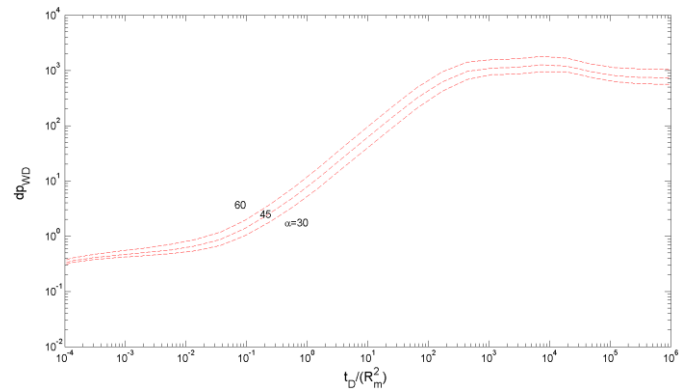

Fig. 9 Effect of the front angle

Formation thickness will affect both the H_D and ε terms. Fig. 10 shows derivative responses generated for different values of $H_D \cdot \varepsilon$ or equivalently H/r_w.

The thicker the formation, the more significant the effect of the gravity becomes. Therefore, a trend similar to that seen in Fig. 9 will appear with longer initial radial flow. In Fig. 10, however, $H_D \cdot \varepsilon$ is used as a correlating parameter and derivatives are divided by this parameter to have identical curves except the deviations for the early time responses.
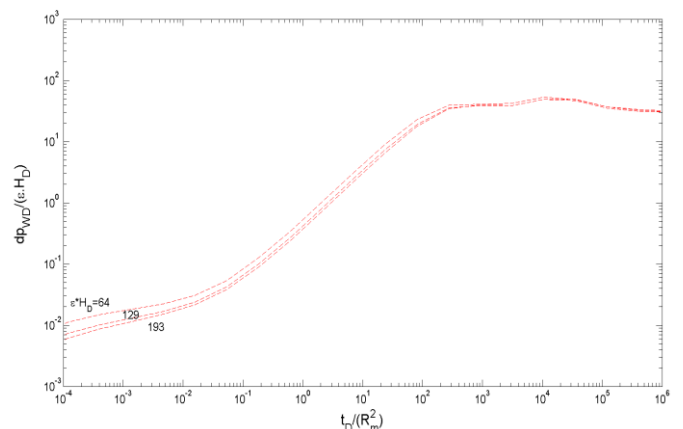

Fig. 10 Effect of formation thickness

3) Effect of the Intermediate Region Size and Properties

Effects of the size of the intermediate region and variation of properties in this region are investigated in this section. Relative size of the intermediate region compared to the inner region, depends on both the minimum front radius (R_m or $R_1´$ in Fig. 1) and front angle, so the correlating parameter in Fig. 11 will be r_{f2}/r_{f1} or more generally the volume ratio.

Fig. 11 shows the effect of the increased size of the intermediate region. Increased size has minor effect on the early response from the intermediate region. However, it highly affects the shape of the transition hump (shown by higher value of maximum derivative and bigger hump) and it will delay the occurrence of the last radial flow corresponding to the outer region.
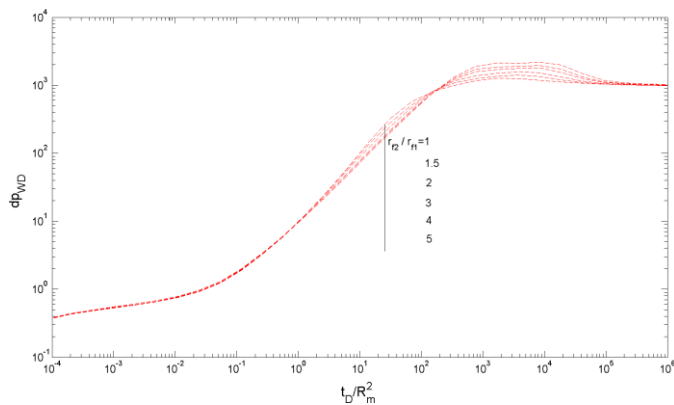

Fig. 11 Effect of the relative size of the intermediate region

Effect of the minimum front radius is shown in Fig. 12. Increased value of R_m or a bigger inner region establishes a longer initial radial flow and the start of the intermediate-region response and the last radial flow are delayed with possible derivative lift due to increased gravity effect.
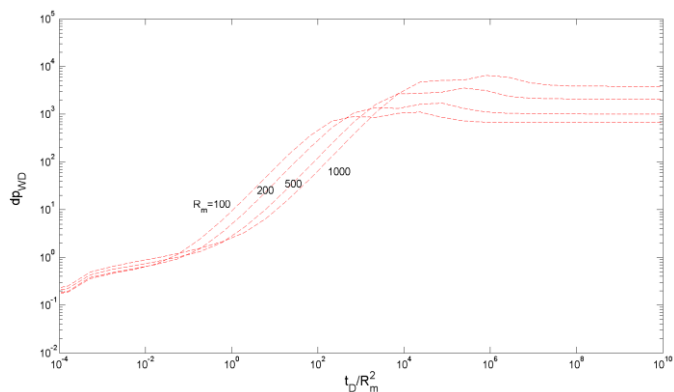

Fig. 12 Effect of the minimum front radius

Effect of the power law variation of mobility and storativity with distance from the first front in the intermediate region are discussed here. Fig. 13 shows that increased value of mobility exponent (θ_1) does not have a significant effect on the shape of the pressure response. However, the observed trend shows less steep intermediate region pressure curves for increased values of θ_1 which means more deviation from the PSS behavior. This is explained by smooth decline of properties in the proposed model, which dampens the sharp property variation assumption of PSS method. Deviation from the PSS behavior is also observed in Fig. 11 with increased size of the intermediate region.
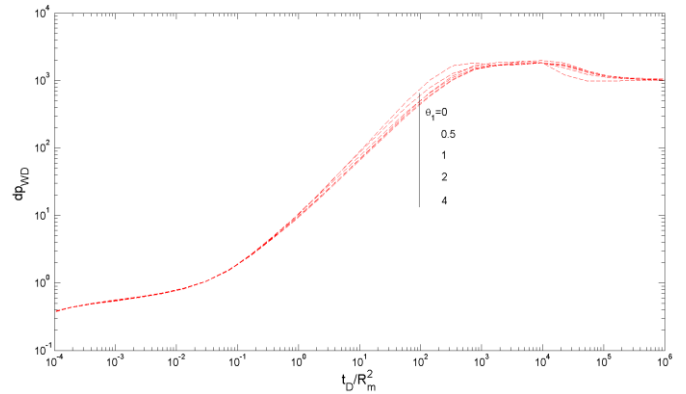

Fig. 13 Effect of the variation of mobility

Fig.14 shows the effect of the storativity exponent (θ_2). This figure supports the trend seen in Fig. 13 that is the deviation from the PSS behavior for smooth property variation. However, it can be stated that the effect of storativity is more significant than the mobility on the shape of the transition hump.

Fig. 14 Effect of the variation of storativity
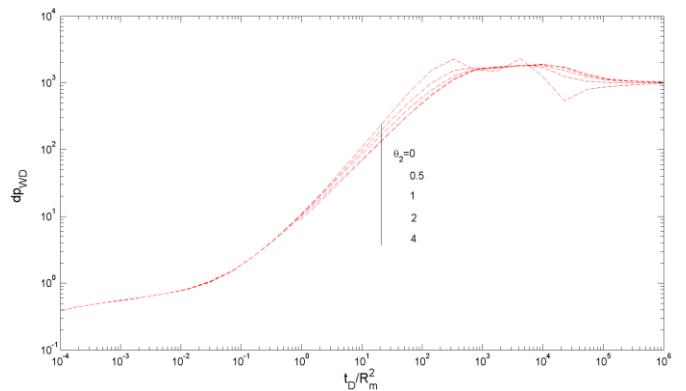
4) Effect of the Boundary Type

The type curves generated and shown so far assume infinite –acting reservoir model. As mentioned in the development of the mathematical model, the solutions for the bounded reservoirs can also be obtained. Fig. 15 shows the pressure and pressure derivative responses for both infinite-acting reservoir and no-flow boundaries. For the closed reservoir

response, pressure and pressure derivative curves converge and show up as unit slope lines on log-log plot indicating the PSS flow behaviour at late times. In the case of constant-pressure boundary (not shown here), pressure derivative declines to zero at late times.
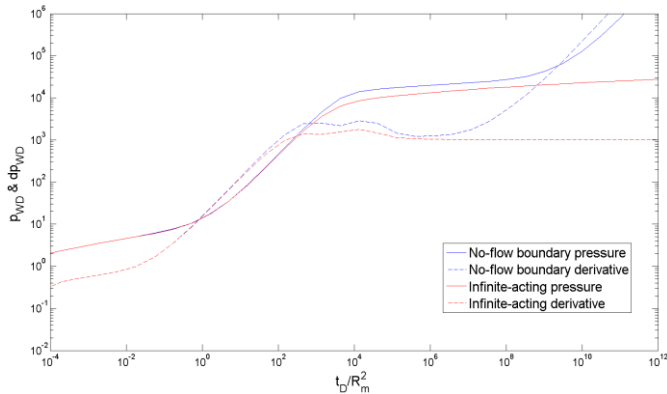

Fig. 15 Comparison of the infinite-acting and no-flow boundary models (r_{eD}=5000000)

IV. CONCLUSIONS

A new general model was developed in this paper, which takes into account some of the assumptions overlooked in the previous models for well test analysis of composite reservoirs. This model was validated against various models in the literature. It explains some of the strange trends seen on the pressure data which are not accounted for by the conventional well test models.

Effect of heat loss (when significant) can highly distort the shape of the pressure response. This can lead to some misinterpretation of the data, as the corresponding heat loss term in the pressure solution has the mathematical form of the linear flow. This term can dominate the flow equations and result in huge estimation errors. Because of the high mobility contrast with the outer region, heat loss does not affect this region and therefore the late time response is not changed.

Mobility and storativity in the intermediate region are assumed to decrease as power law functions of the radial distance from the front. Smooth variation of properties considered in this study will avoid abrupt changes and unrealistic pressure behavior at the front location, which is sometimes assigned a thin skin to account for the phenomena happening at the front.

Sharp vertical fronts seem unrealistic in the case of gravity override or in some cases where viscous fingering happens. Representation of the reservoir model with tilted fronts discussed in this paper is more realistic than the idealization of the traditional two and three-region composite reservoir models with sharp fronts.

Significant effect of gravity can result in longer initial radial flow. It can also cause increase in the value of the late time derivative and the occurrence of the transition hump and the last radial flow may also be delayed. Size and functional variation of properties of the intermediate region considered in this study can affect the shape and occurrence of the transition

zone (in the shape of a hump or maximum based on the model parameters) on the pressure derivative plot.

PSS method is not always appropriate for volume estimations because of its simplifying assumptions. Several parameters implemented in the model in this study such as smooth variation of properties from inner region to outer region and increased size of the intermediate region exhibit deviation from the PSS behavior. It is suggested to consider type curve matching method as an alternative for reservoir characterization based on a general model to be able to obtain better estimates and to explain any anomalies seen on the pressure data.

The model developed in this study offers improvement over the sharp front idealization of the composite reservoir models and can be further extended and applied to other types of EOR processes or reservoirs that can be represented by a composite model such as geothermal reservoirs. The model can also be applied in interference test analysis with arbitrary placement of the observation well in different regions.

NOMENCLATURE

B	Formation volume factor, m^3/Sm^3
c_t	Total compressibility, Pa^{-1}
C_D	Dimensionless wellbore storage coefficient
F	Storativity ratio at the front between different regions
F_ρ	Density ratio of water to steam, dimensionless
G	Rate of steam condensation, $m^3/(s.m^3)$
g	Acceleration of gravity, m/s^2
h	Depth, m
H	Thickness of the reservoir, m
k	Permeability, m^2
K	Thermal conductivity, $W/(m.K)$
M	Mobility ratio at the front between different regions
p	Pressure, Pa
p_D	Dimensionless pressure change
p_i	Initial reservoir pressure, Pa
q	Injection (production) flow rate, Sm^3/s
r	Radial distance, m
r_D	Dimensionless radial distance
s	Laplace variable
S	Skin factor, dimensionless
t	Time, s
t_D	Dimensionless time
T	Temperature, K
T_R	Reservoir temperature, K
T_S	Steam temperature, K

Greek Letters

α	Thermal diffusivity, m^2/sec

α_1	First front angle
α_2	Second front angle
β	Steam condensation coefficient, dimensionless
δ	Density ratio, dimensionless
θ_1	Exponent for mobility variation
θ_2	Exponent for storativity variation
μ	Viscosity, Pa.s
ρ	Density, kg/m^3
φ	Porosity, fraction
Φ	Flow potential, Pa

APPENDIX A: DEVELOPMENT OF THE SOLUTION TO FLOW EQUATION IN THE INTERMEDIATE REGION

A solution to equation 13 is obtained by comparison with the solution for the general Bessel equation. The general Bessel equation in Laplace space is given in [26] as:

$$\frac{d^2\bar{y}}{dx^2} + \frac{n}{x}\frac{d\bar{y}}{dx} - \frac{q^2}{x^{n-m}}\bar{y} = 0$$

A solution to this equation is:

$$\bar{y} = Ax^{-\frac{1}{2}(n-1)}K_v\left(\frac{2q}{m-n+2}x^{-\frac{1}{2}(m-n+2)}\right) + Bx^{-\frac{1}{2}(n-1)}I_v\left(\frac{2q}{m-n+2}x^{-\frac{1}{2}(m-n+2)}\right)$$

Where

$$v = \frac{1-n}{m-n+2}$$

Comparison of equation 13 with the general Bessel equation above yields:

$$\overline{p_{2D}} \equiv \bar{y} \qquad r_D \equiv x \qquad 1 - \theta_1 \equiv n$$

$$\frac{M_{12}}{F_{12}}(R_{1D} - \varepsilon\cot\alpha_1 h_D)^{\theta_2 - \theta_1}s \equiv q^2 \qquad 1 - \theta_2 \equiv m$$

The equivalent solution to equation 13 is therefore:

$$\overline{p_{2D}} = Cr_D{}^\gamma I_v(\xi r_D{}^b) + Dr_D{}^\gamma K_v(\xi r_D{}^b)$$

Where

$$\gamma = \frac{\theta_1}{2} \qquad\qquad b = \frac{\theta_1 - \theta_2 + 2}{2}$$

$$v = \frac{\theta_1}{\theta_1 - \theta_2 + 2} \qquad \xi = \sqrt{\frac{M_{12}}{F_{12}}s}\frac{\sqrt{(R_{1D} - \varepsilon\cot\alpha_1 h_D)^{\theta_2 - \theta_1}}}{b}$$

APPENDIX B: MATRIX OF COEFFICIENTS FOR PRESSURE SOLUTION

Taking Laplace of the boundary conditions introduced in the description of the model, the elements of the matrix of coefficients are written as:

$$a_{11} = \sqrt{s}\,I_1(\sqrt{s})$$
$$a_{12} = -\sqrt{s}\,K_1(\sqrt{s})$$

$$a_{21} = \int_0^{H_D} I_0(\sqrt{s}\,r_{f1D})\,dh_D$$

$$a_{22} = \int_0^{H_D} K_0(\sqrt{s}\,r_{f1D})\,dh_D$$

$$a_{23} = -\int_0^{H_D} r_{f1D}{}^\gamma I_v(\xi\,r_{f1D}{}^b)\,dh_D$$

$$a_{24} = -\int_0^{H_D} r_{f1D}{}^\gamma K_v(\xi\,r_{f1D}{}^b)\,dh_D$$

$$a_{33} = \int_0^{H_D} r_{f2D}{}^\gamma I_v(\xi\,r_{f2D}{}^b)\,dh_D$$

$$a_{34} = \int_0^{H_D} r_{f2D}{}^\gamma K_v(\xi\,r_{f2D}{}^b)\,dh_D$$

$$a_{35} = -\int_0^{H_D} I_0\left(\sqrt{\frac{M_{13}}{F_{13}}s}\,r_{f2D}\right)dh_D$$

$$a_{36} = -\int_0^{H_D} K_0\left(\sqrt{\frac{M_{13}}{F_{13}}s}\,r_{f2D}\right)dh_D$$

$$a_{41} = M_{12}\sqrt{s}\int_0^{H_D} I_1(\sqrt{s}\,r_{f1D})\,dh_D$$

$$a_{42} = -M_{12}\sqrt{s}\int_0^{H_D} K_1(\sqrt{s}\,r_{f1D})\,dh_D$$

$$a_{43} = -\int_0^{H_D}\left[\gamma r_{f1D}{}^{\gamma-1}I_v(\xi\,r_{f1D}{}^b) + \xi b\,r_{f1D}{}^{\gamma+b-1}\acute{I}_v(\xi\,r_{f1D}{}^b)\right]dh_D$$

$$a_{44} = -\int_0^{H_D}\left[\gamma r_{f1D}{}^{\gamma-1}K_v(\xi\,r_{f1D}{}^b) + \xi b\,r_{f1D}{}^{\gamma+b-1}\acute{K}_v(\xi\,r_{f1D}{}^b)\right]dh_D$$

$$a_{53} = M_{23}\int_0^{H_D}\left[\gamma r_{f2D}{}^{\gamma-1}I_v(\xi\,r_{f2D}{}^b) + \xi b\,r_{f2D}{}^{\gamma+b-1}\acute{I}_v(\xi\,r_{f2D}{}^b)\right]dh_D$$

$$a_{54} = M_{23}\int_0^{H_D}\left[\gamma r_{f2D}{}^{\gamma-1}K_v(\xi\,r_{f2D}{}^b) + \xi b\,r_{f2D}{}^{\gamma+b-1}\acute{K}_v(\xi\,r_{f2D}{}^b)\right]dh_D$$

$$a_{55} = -\sqrt{\frac{M_{13}}{F_{13}}s}\int_0^{H_D} I_1\left(\sqrt{\frac{M_{13}}{F_{13}}s}\,r_{f2D}\right)dh_D$$

$$a_{56} = \sqrt{\frac{M_{13}}{F_{13}}s}\int_0^{H_D} K_1\left(\sqrt{\frac{M_{13}}{F_{13}}s}\,r_{f2D}\right)dh_D$$

For infinite-acting reservoir:

$$a_{65} = a_{66} = 0$$

For no-flow boundary:

$$a_{65} = I_1\left(\sqrt{\frac{M_{13}}{F_{13}}s}\,r_{eD}\right)$$

$$a_{66} = -K_1\left(\sqrt{\frac{M_{13}}{F_{13}}s}\,r_{eD}\right)$$

For constant-pressure boundary:

$$a_{65} = I_0\left(\sqrt{\frac{M_{13}}{F_{13}}s}\,r_{eD}\right)$$

$$a_{66} = K_0\left(\sqrt{\frac{M_{13}}{F_{13}}s}\,r_{eD}\right)$$

The elements of matrix *d* are written as:

$$d_1 = -\frac{1}{s}$$

$$d_2 = \frac{H_D{}^2}{2s}\left(\frac{1}{\delta_{12}} - 1\right) - \beta \frac{\sqrt{\pi}}{s^{3/2}} H_D$$

$$d_3 = \frac{H_D{}^2}{2s}\left(\frac{1}{\delta_{13}} - \frac{1}{\delta_{12}}\right)$$

$$d_4 = \frac{\tan\alpha_1 H_D}{\varepsilon\, s}\left(M_{12} - \frac{1}{\delta_{12}}\right)$$

$$d_5 = \frac{\tan\alpha_2 H_D}{\varepsilon\, s}\left(\frac{M_{23}}{\acute\delta_{12}} - \frac{1}{\delta_{13}}\right)$$

$$d_6 = 0$$

REFERENCES

[1] R. D. Carter, "Pressure Behavior of a Limited Circular Composite Reservoir," *SPE J.* vol. 6(4) pp. 328-34, 1966. http://dx.doi.org/10.2118/1621-PA

[2] A. Satman, M. Eggenschwiler, R. W-K. Tang, and H. J. Ramey Jr., "An Analytical Study of Transient Flow in Systems with Radial Discontinuities," in *the 55th Annual Meeting of SPE of AIME, Dallas, Texas*, 21-24 September, 1980, paper SPE 9399. http://dx.doi.org/10.2118/9399-MS

[3] M. O. Onyekonwu, H. J. Ramey Jr., W. E. Brigham, and R. M. Jenkins, "Interpretation of Simulated Falloff Tests," in *the California Regional Meeting of SPE of AIME, Long Beach, California*, 11-13 April, 1984, paper SPE 12746. http://dx.doi.org/10.2118/12746-MS

[4] J. Barua and R. N. Horne, "Computerized Analysis of Thermal Recovery Well Test Data," *SPE Formation Evaluation Journal,* vol. 2(4), pp. 560-66, 1987. http://dx.doi.org/10.2118/12745-PA

[5] A.K. Ambastha and H. J. Ramey Jr., "Pressure Transient Analysis for a Three- Region Composite Reservoir," in *the Rocky Mountain Regional Meeting of SPE of AIME, Casper, Wyoming*, 1992, paper SPE 24378 http://dx.doi.org/10.2118/24378-MS

[6] T. Nanba and R. N. Horne, "Estimation of Water and Oil Relative Permeabilities from Pressure Transient Analysis of Water Injection Well Data," in *the Annual Technical Conference and Exhibition of SPE of AIME, San Antonio, Texas*, 8-11 October, 1989, paper SPE 19829. http://dx.doi.org/10.2118/19829-MS

[7] M. Abbaszadeh and M. Kamal, "Pressure Transient Testing of Water Injection Wells," *SPE Res. Eng.,* vol. 4(1), pp. 115-124, 1989. http://dx.doi.org/10.2118/16744-PA

[8] R. B. Bratvold and R. N. Horne, "Analysis of Pressure Falloff Tests following Cold Water Injection," *SPE Formation Evaluation Journal*, vol. 5(3) pp. 293-302, 1990. http://dx.doi.org/10.2118/18111-PA

[9] L.G. Acosta and A.K. Ambastha, "Thermal Well Test Analysis Using an Analytical Multi-Region Composite Reservoir Model," in *the Annual Technical Conference and Exhibition of SPE of AIME, New Orleans, Louisiana*, September 25-28, 1994, paper SPE 28422 http://dx.doi.org/10.2118/28422-MS

[10] C. Chakrabarty, "Pressure Transient Analysis of Non- Newtonian Power Law Fluid Flow in Fractal Reservoirs," PhD Thesis, University of Alberta, Edmonton, Alberta, April 1993.

[11] D. Poon, "Transient Pressure Analysis of Fractal Reservoirs," in *the Annual Technical Meeting of the Petroleum Society of Canada, Calgary, Alberta*, June 7-9, 1995, paper PETSOC 95-34. http://dx.doi.org/10.2118/95-34

[12] M. B. Issaka and A. K. Ambastha, "An Improved Three-region Composite Reservoir Model for Thermal Recovery Well Test Analysis," in *the Annual Meeting of CIM, Calgary, Alberta*, June 8-11, 1997, paper CIM 97-55. http://dx.doi.org/10.2118/97-55

[13] A. N. Duong, "Thermal Transient Analysis Applied to Horizontal Wells," in *the 2008 SPE international thermal operations and heavy oil symposium, Calgary, Canada*, October 20-23, 2008, paper SPE 117435. http://dx.doi.org/10.2118/117435-MS

[14] L. Zhu, F. Zeng, and G. Zhao, "A Condensation Temperature Model for Evaluating Early-period SAGD Performance," in *the SPE heavy oil conference, Calgary, Canada*, 12-14 June, 2012, paper SPE 157800. http://dx.doi.org/10.2118/157800-MS

[15] L. Zhenyu, H. Jinbao, and W. Huzhen, "A new well test model for two region heavy oil thermal recovery considering gravity override and heat loss," *Petroleum Exploration and Development Journal*, vol. 37 (5) pp. 596-600, 2010. doi:10.1016/S1876-3804(10)60057-2

[16] A. Jahanbani G., T. A. Jelmert, J. Kleppe, M. Ashrafi, Y. Souraki, and O. Torsaeter, "Investigation of the applicability of thermal well test analysis in steam injection wells for Athabasca heavy oil," in *EAGE Annual Conference & Exhibition incorporating SPE Europec, Copenhagen, Denmark*. 4-7 June, 2012, paper SPE 154182. http://dx.doi.org/10.2118/154182-MS

[17] A. Jahanbani G., T. A. Jelmert, J. Kleppe, "Investigation of thermal well test analysis for horizontal wells in SAGD process," in *SPE Annual Technical Conference and Exhibition (ATCE), San Antonio, USA*, 8-10 October, 2012, paper SPE 159680. http://dx.doi.org/10.2118/159680-MS

[18] A. Jahanbani G. and J. Kleppe, "Analysis of Heat Loss Effects on Thermal Pressure Falloff Tests," in *the 14th European Conference on the Mathematics of Oil Recovery, Catania, Sicily, Italy*, 8-11 September, 2014, paper EAGE- Mo P23. DOI: 10.3997/2214-4609.20141806

[19] Y. C. Yortsos, "Distribution of fluid phases within the steam zone in steam-injection processes," *SPE Journal*, vol. 24(4), pp. 458-466, 1984. http://dx.doi.org/10.2118/11273-PA

[20] J. F. Stanislav, C. V. Easwaran, and S. L. Kokal, "Interpretation of thermal well falloff testing," *SPE Formation Evaluation Journal*, vol. 4(2), pp. 181-186, 1989. http://dx.doi.org/10.2118/16747-PA

[21] H. Stehfest, "Algorithm 368: numerical inversion of Laplace transform," *Commun. Assoc. Comput. Math.*, vol. 13(1), pp. 47–49, 1970.

[22] A. F. van Everdingen and W. Hurst, "The application of the Laplace transformation to flow problems in reservoirs," *JPT,* vol. 1(12), pp. 305–324, 1949. http://dx.doi.org/10.2118/949305-G

[23] R. G. Agarwal, R. Al-Hussainy, and H. J. Ramey Jr., "An Investigation of Wellbore Storage and Skin Effect in Unsteady Liquid Flow: I. Analytical Treatment," *SPE Journal*, vol. 10(3), pp. 279-290, 1970. http://dx.doi.org/10.2118/2466-PA

[24] A. K. Ambastha, "Pressure Transient Analysis for Composite Systems," PhD Thesis, Stanford University, Stanford, USA, 1988.

[25] A. Satman, "An Analytical Study of Transient Flow in Stratified Systems with Fluid Banks," in *SPE Annual Technical Conference and Exhibition, San Antonio, Texas*, 4-7 October, 1981, paper SPE 10264. http://dx.doi.org/10.2118/10264-MS

[26] H. S. Carslaw and J. C. Jaeger, *Conduction of Heat in Solids*. London, UK: Oxford University Press, 1959.